NANO LETTERS

pubs.acs.org/NanoLett Letter

Stepwise Enzymatic-Dependent Mechanism of Ebola Virus Binding to Cell Surface Receptors Monitored by AFM

Qingrong Zhang, Jinsung Yang, Sueli Tillieux, Zhengyuan Guo, Rita dos Santos Natividade, Melanie Koehler, Simon Petitjean, Zongqiang Cui, and David Alsteens*

Cite This: https://doi.org/10.1021/acs.nanolett.1c04677 Read Online

ACCESS | Metrics & More | Article Recommendations | Supporting Information

ABSTRACT: Ebola virus (EBOV) is responsible for several outbreaks of hemorrhagic fever with high mortality, raising great public concern. Several cell surface receptors have been identified to mediate EBOV binding and internalization, including phosphatidylserine (PS) receptors (TIM-1) and C-type lectin receptors (DC-SIGNR). However, the role of TIM-1 during early cell surface binding remains elusive and in particular whether TIM-1 acts as a specific receptor for EBOV. Here, we used force−distance curve-based atomic force microscopy (FD-based AFM) to quantify the binding between TIM-1/DC-SIGNR and EBOV glycoprotein (GP) and observed that both receptors specifically bind to GP with high-affinity. Since TIM-1 can also directly interact with PS at the single-molecule level, we also confirmed that TIM-1 acts as dual-function receptors of EBOV. These results highlight the direct involvement of multiple high-affinity receptors in the first steps of binding to cell surfaces, thus offering new perspectives for the development of anti-EBOV therapeutic molecules.

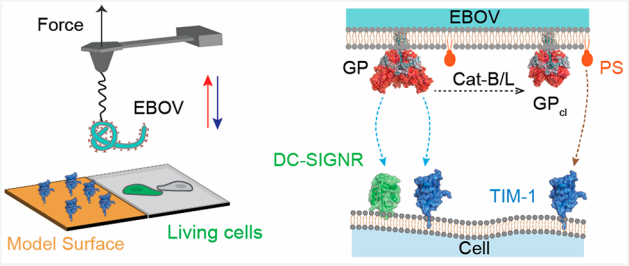

KEYWORDS: *Ebola virus, DC-SIGNR, TIM-1, attachment, cell surface receptor, atomic force microscopy, single-virus force spectroscopy*

Initially discovered in 1976, Ebola virus disease is a severe and often fatal illness affecting humans and other primates.[1] Unlike previous epidemics, the 2014−2016 epidemic spread in West Africa through several countries and is still circulating in several African countries, raising fears of the worst internationally. Among the Ebola various strains, the Zaire Ebolavirus (EBOV) is the most widespread.[2] EBOV is a single-stranded RNA enveloped virus encoding for seven structural proteins[3,4] and possesses a striking filamentous structure. The viral envelope consists of phosphatidylserine (PS)-enriched lipid-bilayer[5] decorated with spikes consisting of the glycoprotein (GP) trimer (Figure 1a).[6] Since last year, a vaccine is available but not suitable for an outbreak response where immediate protection is required. However, currently the poor understanding of cellular receptor role is a major roadblock in the understanding of EBOV pathogenesis and the development of antiviral therapies, needed to treat the disease.

EBOV infects a wide range of host cells[7] and a variety of cell surface receptors have been identified or hypothesized to mediate EBOV binding and internalization into the endosomal compartment of cells, including PS receptors and C-type lectin receptors.[8−10] PS receptors and in particular the T-cell Ig and mucin domain 1 (TIM-1) receptor has been shown to interact with the viral PS,[11,12] mediating GP-independent virus uptake. However, evidence also suggests a direct interaction between TIM-1 and EBOV glycoprotein (EBOV-GP),[13] questioning the exact role of TIM-1 during virus binding and infection. Besides TIM-1, the C-type lectin dendritic cell-specific intercellular adhesion molecule-3-grabbing nonintegrin receptor (DC-SIGNR) has been identified to specifically bind to EBOV-GP contributing to EBOV binding to host cell surface.[14,15] After EBOV attachment to the cell surface, the viral particles are internalized into early endosomes, where GP is cleaved to GP$_{cl}$ by cathepsin-B and cathepsin-L (Cat-B/L) in a low-pH-dependent manner (Figure 1b).[16,17] The GP$_{cl}$ then interacts with the Niemann-Pick C1 receptor triggering membrane fusion.[18] In addition, the GP can be cleaved by the tumor necrosis factor-α converting enzyme (TACE) at the membrane-proximal external region (Figure 1b).[19,20] Overall, the mechanism of molecular binding of EBOV to the cell surface is still unclear, in particular the role of TIM-1 in binding to the GP glycoprotein during attachment of virions to the cell surface.

To clarify the role of human host receptors during early binding events of EBOV to cell surfaces, we used force−distance (FD) curve-based atomic force microscopy (AFM) (Figure 1c)[21] and probed at the single virus-like particle (VLP)

Received: December 3, 2021
Revised: January 30, 2022

https://doi.org/10.1021/acs.nanolett.1c04677
Nano Lett. XXXX, XXX, XXX−XXX

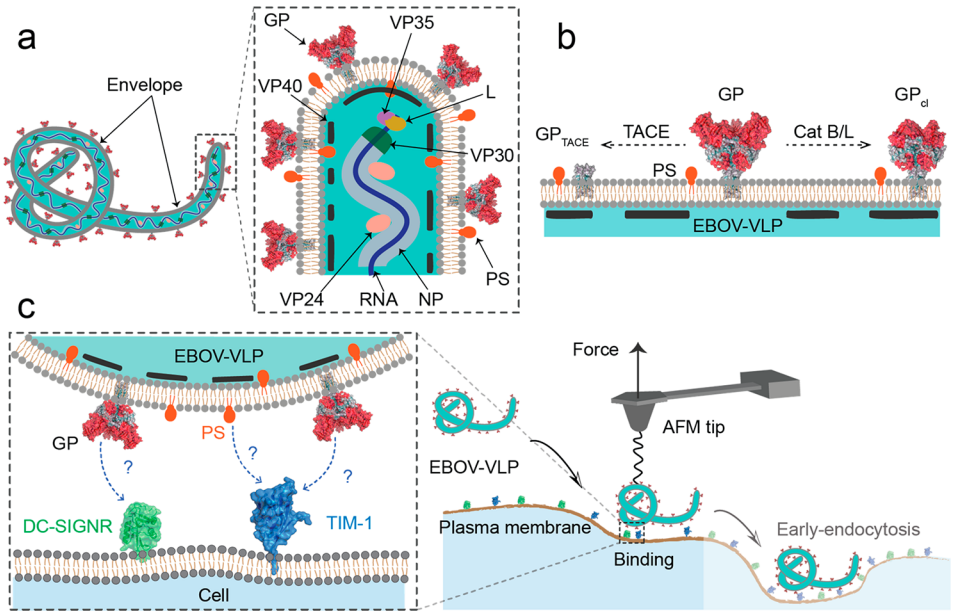

Figure 1. Schematic of EBOV and AFM probing of EBOV binding to living cells. (a) Schematic of EBOV, the nucleoprotein (NP) encases the viral RNA genome to form a protein−RNA complex. The viral RNA genome interacts with the virion-associated proteins VP24, transcriptional activator VP30, polymerase cofactor VP35, and polymerase L. This complex is surrounded by the matrix protein VP40, which is the main protein controlling virion morphology and budding. These inner components are packed in an envelope of lipid bilayer containing phosphatidylserine (PS). The trimers of glycoprotein (GP) spike are embedded in the viral envelope.[4] (b) Schematic of protease cleavages of EBOV-GP. GP is cleaved at a membrane-proximal external region by the tumor necrosis factor-α converting enzyme (TACE). Endosomal cysteine proteases Cat B/L cleaves GP species to generate GP$_{cl}$. (c) Cartoon showing the probing of EBOV-VLP to cell surface receptors, in particular DC-SIGNR and TIM-1 (PDB IDs: DC-SIGNR, 1K9J; TIM-1, 5DZO; GP, 5JQ3).

level, the interactions toward DC-SIGNR and TIM-1 receptors, both on purified receptors and on living cells. We first extracted the kinetics and thermodynamics parameters of the individual interactions and further evaluated the binding capacity of EBOV-receptors on living cells. We evidenced that GP specifically interacts with both DC-SIGNR and TIM-1 with a high-affinity (∼15−20 nM). Treatment with Cat-B/L and TACE also suggests that TIM-1 also interacts with PS, providing the first direct evidence that TIM-1 acts as a dual attachment receptor for EBOV. However, the interaction between TIM-1 and PS mainly occurs after enzymatic cleavage of GP, presumably within the endosome.

RESULTS

EBOV Specifically Binds to Both DC-SIGNR and TIM-1.

To evaluate the role of PS receptors and C-type lectin receptors during EBOV early binding to cell surface, we evaluated the binding potential of EBOV to purified receptors using FD-curve based AFM. To this end, DC-SIGNR or TIM-1 were covalently grafted to gold surfaces coated with COOH- and OH-terminated alkanethiols through carbodiimide conjugation (see Supporting Information (SI) Methods). The grafted surfaces were validated by AFM scratching, showing a deposited layer of ∼1.5 nm and ∼2.0 nm for DC-SIGNR and TIM-1, respectively (Figure S1a,b). EBOV-like particles (EBOV-VLPs) were produced by expressing the EBOV-GP and mCherry-labeled matrix protein VP40 as previously described.[22] Confocal laser-scanning microscopy and AFM imaging were used to validate the production of EBOV-VLPs (Figure S2a,b).

Purified EBOV-VLPs were then covalently immobilized onto the AFM tips using a 24-unit long polyethylene glycol (PEG) spacer and the grafting procedure was validated by confocal laser-scanning microscopy (Figure 2a and Figure S2c,d). In order to evaluate the binding between EBOV-VLPs and both receptors, FD curves were recorded by repeatedly approaching and retracting the functionalized tip from the DC-SIGNR or TIM-1 decorated model surface with a surface delay of 200 ms (Figure 2a,b and Figure S3). Specific binding events were observed in 16.3 ± 1.6% and 33.5 ± 2.9% of retraction FD curves for DC-SIGNR and TIM-1, respectively (Figure 2c). To confirm the binding specificity, several independent controls were performed using (i) an coated OH-/COOH-terminated alkanethiol coated surfaces lacking the individual receptors, (ii) a tip functionalized with the PEG spacer but no EBOV-VLPs, and (iii) the injection of 10 nM free antibodies (Ab) (DC-SIGNR Ab or TIM-1 Ab). All three controls result in a significant drop of the binding probability (BP), confirming the specificity of the probed interaction between EBOV-VLPs and DC-SIGNR or TIM-1 (Figure 2c).

TIM-1 Binds Both PS and EBOV-GP. In order to identify which EBOV ligands are involved in host receptor binding, we combined the use of native and protease-treated virions yielding different forms of cleaved EBOV-GP. Using FD-curve-based AFM, we compared the BP of the interaction between EBOV-VLP and DC-SIGNR before and after treatment with CatB/L or TACE proteases (Figure S4). We observed significant drops in the BP after each protease treatment (Figure 2d) from 16.3 ± 1.6% before treatment to 8.5 ± 0.7% and 7.2 ± 0.2% using CatB/L or TACE treatments, respectively (Figure 2d). The low BP observed after the protease treatment is also very close to the value obtained after blocking with DC-SIGNR-Ab, suggesting that no other viral surface component is involved in the binding to DC-SIGNR.

Similarly, we evaluated the role of EBOV-GP and PS as potential binding ligands for TIM-1. Using Annexin-V, known

https://doi.org/10.1021/acs.nanolett.1c04677
Nano Lett. XXXX, XXX, XXX−XXX

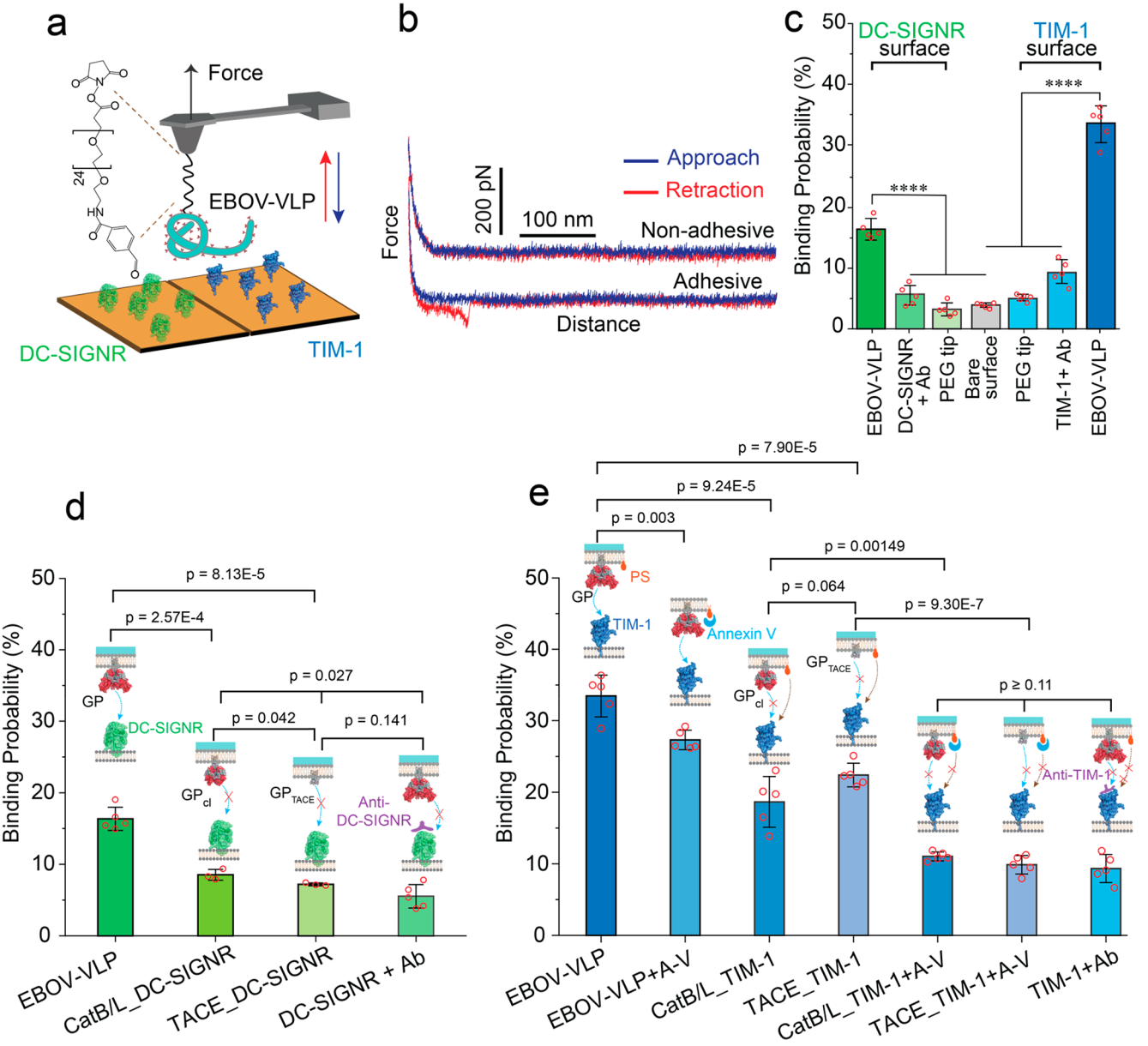

Figure 2. EBOV-VLPs specifically binds to purified receptors. (a) Schematic of the functionalized of the AFM tip with a PEG_{24} spacer that grafted to the free amino group of EBOV-VLP or GP. (b) Representative FD curves recorded on the model surface showing nonadhesion and specific adhesion event. (c) Binding probabilities (BP) of specific adhesion events recorded between EBOV-VLP and different receptors and measured by AFM. Red circle indicates individual data points (extracted from independent individual maps), the box indicates the mean, and whiskers indicate the mean ± standard deviation (s.d.). (d,e) The BP of EBOV-VLP binding to DC-SIGNR (d) or TIM-1 (e) before or after treatment with TACE, CatB/L proteases, Annexin-V, and TIM-1 Ab. All experiments were independently reproduced at least three times ($n \geq 3$). **** $P < 0.0001$, P values were determined by a two-sample t test using Origin. Error bars indicate s.d. of mean.

to specifically bind to PS, we only observed a small decrease of the BP (from 33.5 ± 2.9% to 27.3 ± 1.5%, $n = 5$), suggesting that PS is poorly accessible to TIM-1 on native EBOV-VLP. After treatment with CatB/L or TACE, the BP significantly decreased (from 33.5 ± 2.9% before treatment to 18.6 ± 3.5% and 22.4 ± 1.6% using CatB/L or TACE, respectively), confirming that EBOV-GP is directly involved in TIM-1 binding, as previously suggested[13,23] (Figure 2e). However, the BP remained largely above the value observed after blocking with TIM-1 Ab, confirming that PS and GP could act as a second-attachment ligand. To further validate this, we treated the EBOV-VLPs with each protease and further incubated them with Annexin-V. For both proteases, the coincubation with Annexin-V resulted in a further drop of the BP to the same level as that observed for the incubation with TIM-1 Ab (Figure 2e). Taken together, these experiments identify TIM-1 as a cellular receptor interacting with both EBOV-GP and PS, while DC-SIGNR exclusively interacts with EBOV-GP.

Extracting the Binding Free-Energy Landscape of EBOV to Cell Surface Receptors. After having identified DC-SIGNR and TIM-1 as cellular receptors for EBOV, we sought to characterize their kinetic and thermodynamic properties (Figure 3a,b) via force-probing their interactions at various loading rates (Figure 3c). Experimentally, the EBOV-VLP functionalized tip is approached at a constant speed toward the functionalized surface and maintained in

https://doi.org/10.1021/acs.nanolett.1c04677
Nano Lett. XXXX, XXX, XXX−XXX

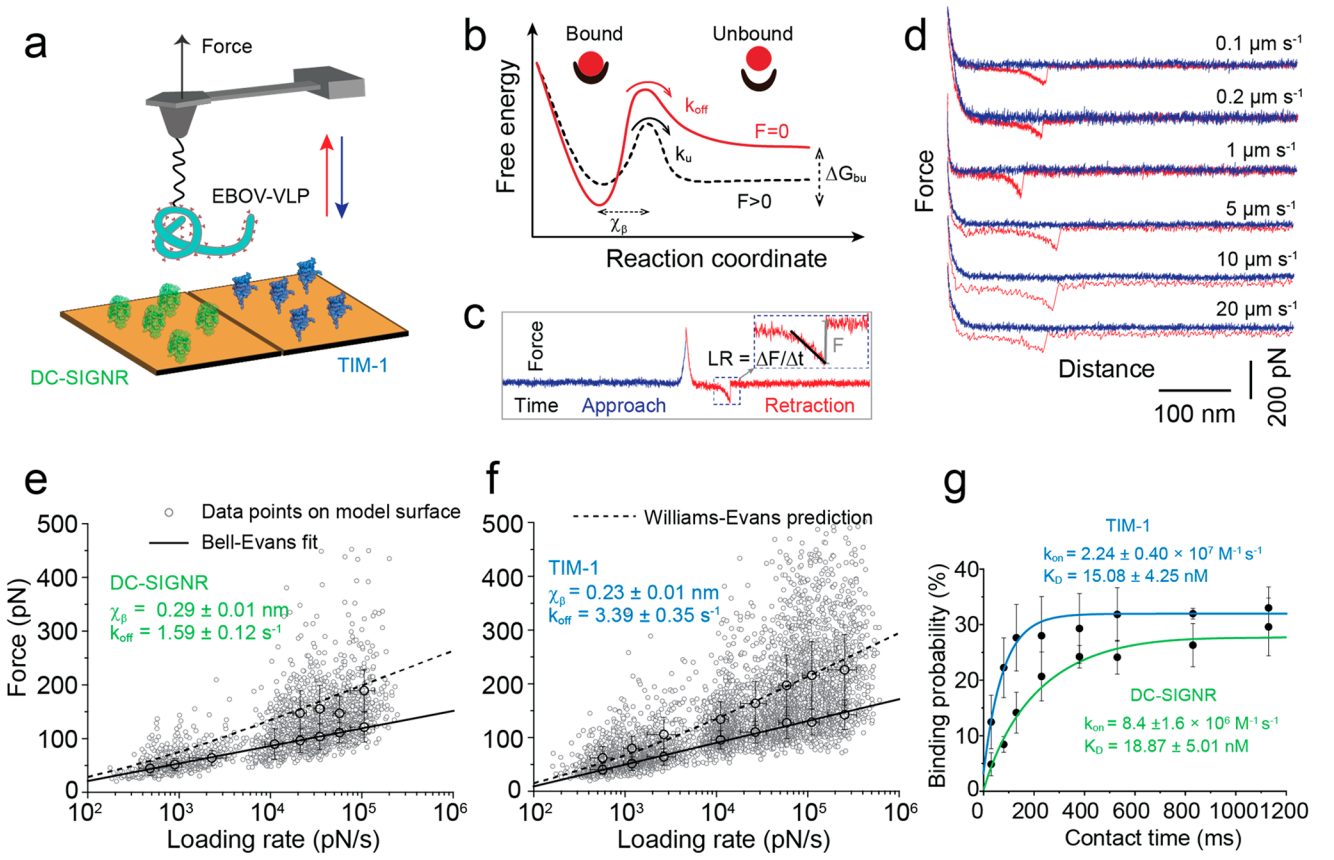

Figure 3. Probing EBOV-VLP binding to receptors on model surface. (a) Cartoon showing the probing of EBOV-VLPs to DC-SIGNR and TIM-1 receptors on the model surface and EBOV-VLPs on AFM tip. (b) Binding between a ligand and a receptor can be described as a two-state by the Bell-Evans model. The transition from the bound state to the unbound state is separated by an energy barrier located at distance χ_β. k_{off}, and k_u indicate the dissociation rate observe with no external force ($F = 0$) or an external force $F > 0$ applied onto the bond. (c) Force versus time curve where the slope of the curve extracted just before the unbinding event is determined to extract the loading rate (LR). (d) Representative force−distance curves recorded at various retraction speeds (from 0.1 to 20 μm s^{-1}) on model surface and showing specific adhesion events. (e,f) Dynamic force spectroscopy (DFS) plot indicating the distribution of the rupture forces at different LR ranges for interactions between EBOV-VLP and DC-SIGNR (n = 2242 data points) (e) or TIM-1 (n = 5220 data points) (f). The solid line represents the fit of the single-bond rupture events with the Bell-Evans fit, giving k_{off} and χ_β values. Dashed lines represent the prediction of the force for the rupture of two simultaneous uncorrelated interactions (using the Williams-Evans prediction). (g) The BP acquired at 1 μm s^{-1} is plotted as a function at the different contact times. A monoexponential decay curve (line) using the least-squares fit provides access to the k_{on} of the probed interactions. K_D (k_{off}/k_{on}) value shows that EBOV-VLP has a higher affinity for DC-SIGNR and TIM-1. All experiments were reproduced three times with independent tips and samples ($n \geq 3$) at least and the error bar shows s.d. of the mean value.

contact for 200 ms, thus allowing the establishment of the bond formation. Next, the tip is retracted at various speeds in the range of 0.1−20 μm s^{-1} (Figure 3d). From the individual force versus time curves (Figure 3c), the rupture force and corresponding loading rate (LR, slope of the curve just before the rupture occurs) were extracted and displayed as individual data points on the dynamic force spectroscopy (DFS) plots (Figure 3e,f). If an external force is applied on a reversible bond, the activation-energy barrier of the molecular bond is reduced toward dissociation and shortens its lifetime as described by Bell-Evans model (Figure 3b).[24,25] In the far-from-equilibrium regime, the model therefore predicts that the rupture force of the bonded molecule pairs is proportional to the logarithm of the LR, as we observe for both receptors (Figure 3e,f).

For both DC-SIGNR and TIM-1, the probed interaction forces are in the range of 25−500 pN in the comprised LR range from 10^2 to 10^6 pN s^{-1} (Figures S5 and 6). The analysis of narrow LR ranges revealed force distributions that follow a multiple Gaussian peak distribution, suggesting the establishment of multiple bonds. For each peak, the average force was extracted and displayed on the respective DFS plots (Figure 3e,f). As predicted by the Bell-Evans model, the points for the first peaks extracted from the histograms were following a linear trend onto the DFS plot (solid lines in Figure 3e,f), enabling to extract their kinetics parameters, i.e., the distance to the transition state (χ_β) and the kinetic off-rate (k_{off}). The binding of the EBOV-VLP to both receptors is described by a single energy barrier with χ_β = 0.29 ± 0.01 nm and k_{off} = 1.59 ± 0.12 s^{-1} for DC-SIGNR, and χ_β = 0.23 ± 0.01 nm and k_{off} = 3.39 ± 0.35 s^{-1} for TIM-1, which is in good agreement with previous work.[26] The k_{off} is directly related to the bond lifetime τ (the time interval required for bond dissociation under equilibrium conditions, $\tau = 1/k_{off}$), which is commonly used to describe the intrinsic parameter of the bond mechanical stability. Our results give lifetimes of $\tau \approx 630$ ms and $\tau \approx 300$ ms for the bond established between EBOV-VLP and DC-SINGR or TIM-1, respectively. These results reveal a two-fold-higher stability for the binding to DC-SIGNR, probably explained by the EBOV tropism as DC-SIGNR is expressed in

https://doi.org/10.1021/acs.nanolett.1c04677
Nano Lett. XXXX, XXX, XXX−XXX

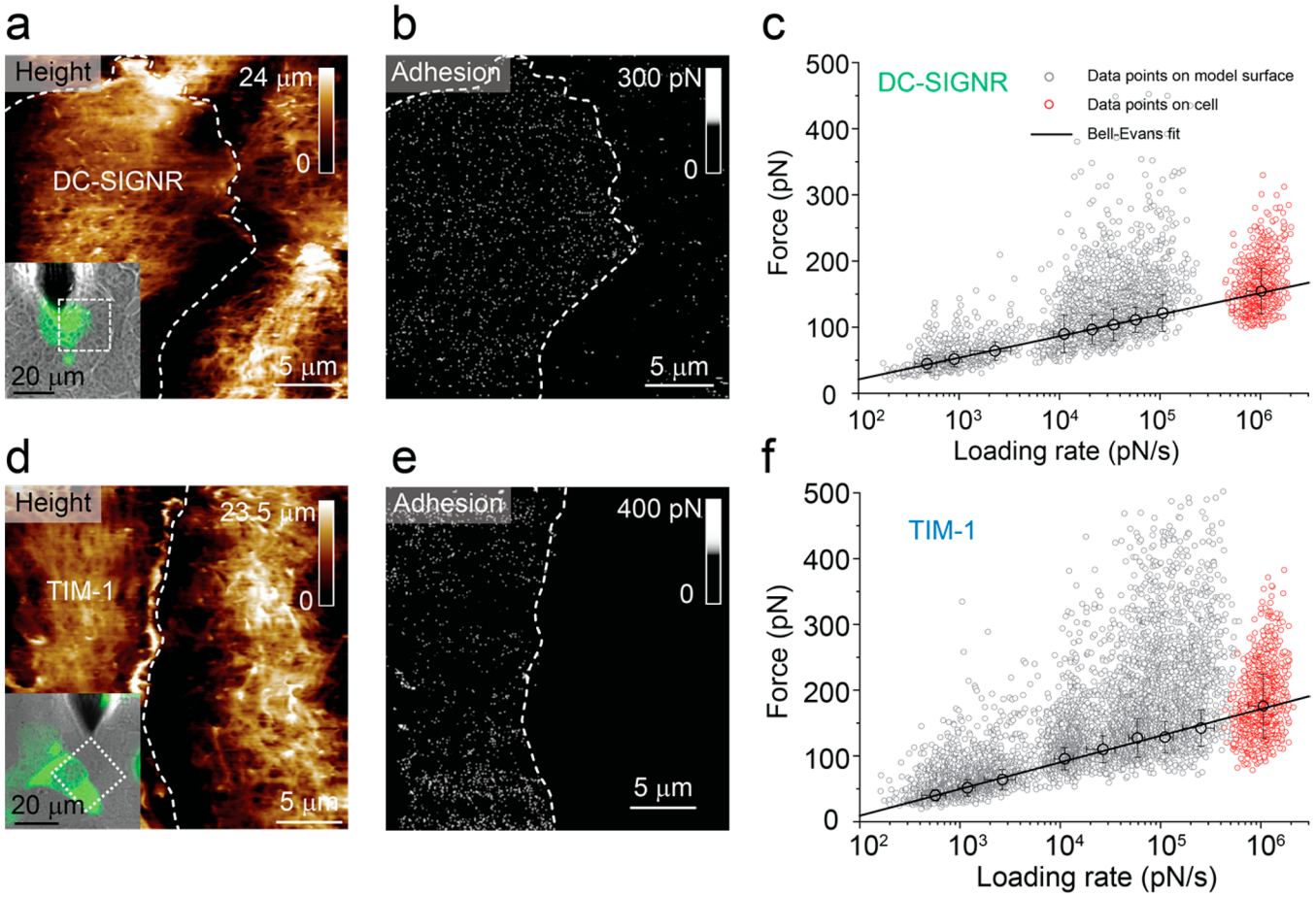

Figure 4. Exploring EBOV-VLPs binding to DC-SIGNR or TIM-1 on living cells. (a) AFM height image of two adjacent HEK 293T cells: DC-SIGNR (fluorescently tagged) cell and an unlabeled negative control cell. Inset: overlay of fluorescent and DIC images of both cells. (b) FD-based AFM adhesion map of cells recorded in the dashed square shown in (a) (inset). (c) DFS plots of data obtained using model surfaces (gray circles, from Figure 3d) and on living cells (red circles, n = 778 data points from three independent experiments). (d) AFM height image with fluorescence image in the inset showing the TIM-1 cell (green) and an unlabeled negative control cell. (e) Corresponding adhesion map recorded with EBOV-VLPs. EBOV-VLPs bind strongly to TIM-1 cells (green) in comparison to the unlabeled cell shown in (d) (inset). (f) DFS plots of TIM-1-EBOV-VLPs obtained using model surfaces (gray circles, from Figure 3e) and on living cells (red circles, n = 908 data points from three independent experiments).

several early targets for EBOV infection, including dendritic cells, alveolar macrophages, and sinusoidal endothelial cells in the liver and lymph node.[14]

Analysis of the rupture forces also revealed higher forces in the DFS plot (Figure 3e,f) and respective force histograms (Figures S5 and 6), which can be fitted with a second peak within the multiple Gaussian peak distribution. Further analysis using the predictive Williams-Evans model,[27,28] which determines whether these higher forces could originate from multiple uncorrelated bonds loaded in parallel between the EBOV-VLPs and the receptors, suggests no particular mechanical coupling between the individual bonds (Figure 3e,f, dashed curves).

Assuming that the receptor-bond complexes can be approximated by a pseudo-first-order kinetics, we also estimated the kinetic on-rate (k_{on}) from our single-molecule force spectroscopy experiments.[29] This association rate is extracted from the BP measured at various contact times and depends on the effective concentration described as the number of binding partners (ligand + receptor) within an effective volume V_{eff} accessible under free-equilibrium interaction. V_{eff} can be approximated by a half-sphere with a radius including the linker, the viral GP and the receptors (see SI Methods).[29,30] For both DC-SIGNR and TIM-1, we observed that the BP increased exponentially with contact time, and we extracted interaction times of ~200 and 80 ms, leading to k_{on} values of 8.4 ± 1.6 × 10^6 M^{-1} s^{-1} and 2.2 ± 0.4 × 10^7 M^{-1} s^{-1}, respectively (Figure 3g). Finally, the dissociation constant K_D is calculated as the ratio between k_{off} and k_{on}, yielding values around ~15–20 nM for both complexes, which is close to the ~26 nM affinity found previously for EBOV-GP−DC-SIGNR.[31] These experiments demonstrate that EBOV-VLP can specifically bind to both DC-SIGNR and TIM-1 via high-affinity interactions in vitro.

TIM-1 Acts as the First Foothold for EBOV-GP Binding. While our first experiments on purified proteins revealed that EBOV-VLPs can bind to TIM-1 through both GP and PS (after cleavage by the proteases), the extraction of the kinetics and thermodynamics revealed only one type of interaction. Therefore, we aimed to determine whether this interaction, recorded with native EBOV-VLPs, originated from binding to EBOV-GP. To this end, we functionalized the AFM tip with the purified EBOV-GP and probed the interaction to both DC-SIGNR and TIM-1 (Figure S7, Table S1). As

https://doi.org/10.1021/acs.nanolett.1c04677
Nano Lett. XXXX, XXX, XXX−XXX

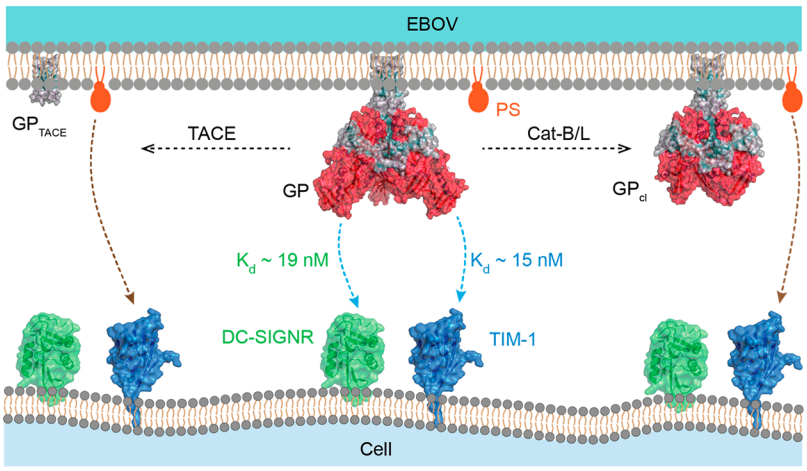

Figure 5. Multiple receptors mediate EBOV binding to host cells with high affinity. Models of EBOV binding to receptors: GP mediates EBOV high-affinity binding to DC-SIGNR and TIM-1. Binding to PS is sterically hindered during the early binding step.

anticipated, for DC-SIGNR we obtained a very good agreement between the parameters extracted using the EBOV-VLPs compared to the one using the purified GP (Figure S7b,c). Stunningly, this is also the case for the complex GP-TIM-1, implying that the EBOV-VLPs would mainly interact with TIM-1 through its GP during the early binding events (Figure S7d,e). This also indicates that binding to PS may occur later during the subsequent step of the infection. Since GP, due to its size, can potentially sterically hinder PS binding, this step could only take place further downstream, once GP is cleaved by CatB/L, just before its internalization into the endosomes.[32]

Exploring EBOV-VLPs Binding to Cellular Receptors on Living Cells. After the extraction of the parameters describing the binding free-energy landscape of EBOV to its cellular receptors on purified receptors, we wanted to further validate that these binding events are also established in a cellular context. To this end, HEK-293T cells were first transiently transfected with DC-SIGNR-GFP. The expression of DC-SIGNR on HEK-293T cells was validated using in-cell-western assays (Figure S8). Next, HEK-293T and HEK-293T-DC-SIGNR-GFP were cocultured and imaged using AFM tips functionalized with EBOV-VLPs under physiologically relevant conditions (37 °C, 95% relative humidity and 5% CO_2) (Figure 4a, inset).[33] Guided by fluorescence, an area where control and transfected cells were adjacent was selected and imaged. This allowed us to directly assess the proportion of specific interactions to a particular receptor compared to other interactions that might be established with constitutively expressed receptors at the cell surface (Figure 4a,b,d,e). From the adhesion map (Figure 4b), a clear difference appears between the control and transfected cells. While control cells show only rare adhesion events (bright pixels, ~1.5%), the transfected cells show a much higher density of adhesion events (~9.3%), homogeneously distributed on the cell surface (Figure 4a,b).

Typical FD curves between EBOV-VLP and HEK-293T-DC-SIGNR-GFP cells showed specific adhesion events on the retraction curve (Figure S9) with rupture forces in the range of 100 to 300 pN across the applied LR range (Figure S9b). Naturally, due to the PEG spacer, the size of the attached EBOV-VLPs, and the elasticity of the cell surface and rupture distances can exceed 200 nm. Overlay of the data on the DFS plot obtained for the purified DC-SIGNR reveals that the binding force for the single-bond matches very well with the value predicted from our above experiments (Figure 4c). Strikingly, despite the short contact time of ~1 ms with the cell surface, specific binding events with DC-SIGNR are established even in a complex cellular environment. Together, these results indicate that EBOV-VLP interacts with DC-SIGNR on cell surfaces using similar high-affinity interactions as measured on model surfaces.

Similarly, we evaluated the binding of EBOV-VLPs to TIM-1 in the cellular context by transiently transfecting HEK-293T with TIM-1-GFP, and we evaluated its functional expression (Figure S10a,b). FD-based AFM using AFM tip derivatized with the EBOV-VLPs revealed that most adhesion events are localized on the transfected cells (Figure 4d,e). Analysis of the rupture force (Figure S11) and comparison with the data extracted on purified TIM-1 (Figure 4f) confirmed that EBOV binds to TIM-1 within a short contact time with the cell surface. The live cell data set clearly shows that EBOV has the ability to rapidly engage with the DC-SIGNR and the TIM-1 receptors immediately after landing on the cell surface, confirming that these two receptors play an important role in infection.

DISCUSSION

EBOV entry requires the concerted action of multiple membrane receptors in the host, including two types of receptors, namely C-type lectin receptors and PS receptors.[34] After binding to the cell surface, EBOV is internalized into the endosomes through the macropinocytosis pathway.[35] Subsequently, the GP is cleaved to trigger the membrane fusion at the endosomes.[36,37] Among PS receptors, the role of TIM-1 remains elusive and is controversially discussed in the literature. A recent study highlights a role for TIM-1 in PS binding during the cellular attachment, allowing it to better resist external mechanical perturbations,[26] whereas another study suggests that TIM-1 serves as a receptor via a direct interaction with EBOV-GP.[13]

Using single-virus force spectroscopy, we investigated EBOV binding to both DC-SIGNR and TIM-1 by quantifying the binding strength to each receptor in vitro on model surfaces and on living cells, mimicking physiologically relevant conditions. We demonstrated that both DC-SIGNR and

https://doi.org/10.1021/acs.nanolett.1c04677
Nano Lett. XXXX, XXX, XXX−XXX

TIM-1 are specific receptors for EBOV early binding to cellular surfaces. The kinetic and thermodynamic investigations pointed out that EBOV-GP specifically binds to DC-SIGNR/TIM-1 with remarkable high affinity (K_D in the nM range, Figure 5). Similar experiments conducted with the purified GP leads to the same conclusion, undoubtedly confirming a direct interaction.

For the first time, we studied at the single virion-level, how enzymes trigger change at the virion surface and how it influences binding properties to cell surface receptors. After EBOV attachment to the cell surface, the viral particles can be cleaved by Cat-B/L and/or TACE. We used AFM to understand how virus binding properties are modified upon enzymes processing. After GP cleavage in the membrane-proximal external region by TACE, we observed that EBOV-VLP still binds to TIM-1. This binding can be impeded by the injection of Annexin-V, suggesting that TIM-1 binding to PS is promoted after enzymatic cleavage. Binding of TIM-1 to PS is also observed after cleavage by Cat-B/L under low-pH conditions with a slightly lower frequency compared to TACE treatment (Figure 2e). Together, these results strikingly demonstrate that TIM-1 acts as a dual-receptor to both EBOV-GP and PS with the latter being favored after enzymatic cleavage within the endosomes.[17]

Findings reported here elucidate the complex interplay between EBOV and its cellular receptors prior to viral entry. Binding of EBOV-GP to TIM-1 and DC-SIGNR serves as the initial high-affinity binding just before the cellular entry. Then, under the action of Cat-B/L and TACE enzymes during endocytosis EBOV-GP is partially cleaved and the TIM-1 receptors present will be able to bind specifically to the PS, thus promoting the membrane fusion step (Figure 5). This two-step entry mechanism, orchestrated by a single cellular receptor, demonstrates the complexity and elegance of the EBOV infection mechanism. This important result points directly to the key role of the TIM-1 receptor making it an ideal candidate for the development of targeted antiviral molecules.

■ ASSOCIATED CONTENT

Supporting Information

The Supporting Information is available free of charge at https://pubs.acs.org/doi/10.1021/acs.nanolett.1c04677.

Additional experimental details, materials, methods, Supplementary Figures 1−11, and Table S1 (PDF)

■ AUTHOR INFORMATION

Corresponding Author

David Alsteens − *Louvain Institute of Biomolecular Science and Technology, Université Catholique de Louvain, Louvain-la-Neuve 1348, Belgium; Walloon Excellence in Life sciences and Biotechnology (WELBIO), Wavre 1300, Belgium;* orcid.org/0000-0001-9229-113X; Email: david.alsteens@uclouvain.be

Authors

Qingrong Zhang − *Louvain Institute of Biomolecular Science and Technology, Université Catholique de Louvain, Louvain-la-Neuve 1348, Belgium*

Jinsung Yang − *Louvain Institute of Biomolecular Science and Technology, Université Catholique de Louvain, Louvain-la-Neuve 1348, Belgium*

Sueli Tillieux − *Louvain Institute of Biomolecular Science and Technology, Université Catholique de Louvain, Louvain-la-Neuve 1348, Belgium*

Zhengyuan Guo − *State Key Laboratory of Virology, Wuhan Institute of Virology, Center for Biosafety Mega-Science, Chinese Academy of Sciences, Wuhan 430071, China*

Rita dos Santos Natividade − *Louvain Institute of Biomolecular Science and Technology, Université Catholique de Louvain, Louvain-la-Neuve 1348, Belgium*

Melanie Koehler − *Louvain Institute of Biomolecular Science and Technology, Université Catholique de Louvain, Louvain-la-Neuve 1348, Belgium;* orcid.org/0000-0003-3042-1749

Simon Petitjean − *Louvain Institute of Biomolecular Science and Technology, Université Catholique de Louvain, Louvain-la-Neuve 1348, Belgium*

Zongqiang Cui − *State Key Laboratory of Virology, Wuhan Institute of Virology, Center for Biosafety Mega-Science, Chinese Academy of Sciences, Wuhan 430071, China;* orcid.org/0000-0003-1564-272X

Complete contact information is available at: https://pubs.acs.org/10.1021/acs.nanolett.1c04677

Author Contributions

Q.Z. and D.A. conceived the project. Q.Z conducted all experiments. Q.Z., J.Y., M.K., R.N., and S.P. analyzed the AFM data. J.Y. and S.T. planned the biochemical experiments and analyzed the data. G.Z. and Z.C. conceived and guided the virus-like particles synthesis and receptor expression. All authors wrote the manuscript.

Notes

The authors declare no competing financial interest.

■ ACKNOWLEDGMENTS

This work was supported by the Université Catholique de Louvain and the Fonds National de la Recherche Scientifique (FRS-FNRS). This project received funding from the European Research Council under the European Union's Horizon 2020 research and innovation program (Grant Agreement 758224) and from the FNRS-Welbio (Grant # CR-2019S-01). The funders had no role in study design, data collection and analysis, decision to publish, or preparation of the manuscript. S.P., M.K., and D.A. are a research fellow, postdoctoral researcher, and research associate at the FNRS, respectively. Q.Z. and D.A. are grateful to China Scholarship Council.

■ REFERENCES

(1) Jacob, S. T.; Crozier, I.; Fischer, W. A.; Hewlett, A.; Kraft, C. S.; Vega, M.-A. de L.; Soka, M. J.; Wahl, V.; Griffiths, A.; Bollinger, L.; Kuhn, J. H. Ebola Virus Disease. *Nat. Rev. Dis. Primers* **2020**, *6* (1), 13.

(2) Feldmann, H.; Geisbert, T. W. Ebola Haemorrhagic Fever. *Lancet* **2011**, *377* (9768), 849−862.

(3) Hoenen, T.; Groseth, A.; Feldmann, H. Therapeutic Strategies to Target the Ebola Virus Life Cycle. *Nat. Rev. Microbiol.* **2019**, *17* (10), 593−606.

(4) Choi, J. H.; Croyle, M. A. Emerging Targets and Novel Approaches to Ebola Virus Prophylaxis and Treatment. *BioDrugs* **2013**, *27* (6), 565−583.

(5) Adu-Gyamfi, E.; Johnson, K. A.; Fraser, M. E.; Scott, J. L.; Soni, S. P.; Jones, K. R.; Digman, M. A.; Gratton, E.; Tessier, C. R.; Stahelin, R. V. Host Cell Plasma Membrane Phosphatidylserine Regulates the Assembly and Budding of Ebola Virus. *J. Virol.* **2015**, *89*, 9440−9453.

(6) Lee, J. E.; Saphire, E. O. Ebolavirus Glycoprotein Structure and Mechanism of Entry. *Future Virol.* **2009**, *4* (6), 621−635.
(7) Martines, R. B.; Ng, D. L.; Greer, P. W.; Rollin, P. E.; Zaki, S. R. Tissue and Cellular Tropism, Pathology and Pathogenesis of Ebola and Marburg Viruses. *J. Pathol.* **2015**, *235* (2), 153−174.
(8) Bhattacharyya, S.; Hope, T. J. Cellular Factors Implicated in Filovirus Entry. *Adv. Virol.* **2013**, *2013*, 1.
(9) Takada, A. Filovirus Tropism: Cellular Molecules for Viral Entry. *Frontiers in Microbiology* **2012**, *3*, 34.
(10) Moller-Tank, S.; Maury, W. Ebola Virus Entry: A Curious and Complex Series of Events. *PLoS Pathog.* **2015**, *11* (4), e1004731.
(11) Moller-Tank, S.; Kondratowicz, A. S.; Davey, R. A.; Rennert, P. D.; Maury, W. Role of the Phosphatidylserine Receptor TIM-1 in Enveloped-Virus Entry. *J. Virol.* **2013**, *87* (15), 8327−8341.
(12) Jemielity, S.; Wang, J. J.; Chan, Y. K.; Ahmed, A. A.; Li, W.; Monahan, S.; Bu, X.; Farzan, M.; Freeman, G. J.; Umetsu, D. T.; DeKruyff, R. H.; Choe, H. TIM-Family Proteins Promote Infection of Multiple Enveloped Viruses through Virion-Associated Phosphatidylserine. *PLoS Pathog.* **2013**, *9* (3), e1003232.
(13) Kondratowicz, A. S.; Lennemann, N. J.; Sinn, P. L.; Davey, R. A.; Hunt, C. L.; Moller-Tank, S.; Meyerholz, D. K.; Rennert, P.; Mullins, R. F.; Brindley, M.; Sandersfeld, L. M.; Quinn, K.; Weller, M.; McCray, P. B.; Chiorini, J.; Maury, W. T-Cell Immunoglobulin and Mucin Domain 1 (TIM-1) Is a Receptor for Zaire Ebolavirus and Lake Victoria Marburgvirus. *Proc. Natl. Acad. Sci. U. S. A.* **2011**, *108*, 8426−8431.
(14) Simmons, G.; Reeves, J. D.; Grogan, C. C.; Vandenberghe, L. H.; Baribaud, F.; Whitbeck, J. C.; Burke, E.; Buchmeier, M. J.; Soilleux, E. J.; Riley, J. L.; Doms, R. W.; Bates, P.; Pöhlmann, S. DC-SIGN and DC-SIGNR Bind Ebola Glycoproteins and Enhance Infection of Macrophages and Endothelial Cells. *Virology* **2003**, *305* (1), 115−123.
(15) Alvarez, C. P.; Lasala, F.; Carrillo, J.; Muñiz, O.; Corbí, A. L.; Delgado, R. C-Type Lectins DC-SIGN and L-SIGN Mediate Cellular Entry by Ebola Virus in Cis and in Trans. *J. Virol.* **2002**, *76*, 6841−6844.
(16) Schornberg, K.; Matsuyama, S.; Kabsch, K.; Delos, S.; Bouton, A.; White, J. Role of Endosomal Cathepsins in Entry Mediated by the Ebola Virus Glycoprotein. *J. Virol.* **2006**, *80* (8), 4174.
(17) Chandran, K.; Sullivan, N. J.; Felbor, U.; Whelan, S. P.; Cunningham, J. M. Endosomal Proteolysis of the Ebola Virus Glycoprotein Is Necessary for Infection. *Science* **2005**, *308* (5728), 1643.
(18) Côté, M.; Misasi, J.; Ren, T.; Bruchez, A.; Lee, K.; Filone, C. M.; Hensley, L.; Li, Q.; Ory, D.; Chandran, K.; Cunningham, J. Small Molecule Inhibitors Reveal Niemann−Pick C1 Is Essential for Ebola Virus Infection. *Nature* **2011**, *477* (7364), 344−348.
(19) Dolnik, O.; Volchkova, V.; Garten, W.; Carbonnelle, C.; Becker, S.; Kahnt, J.; Ströher, U.; Klenk, H.-D.; Volchkov, V. Ectodomain Shedding of the Glycoprotein GP of Ebola Virus. *EMBO J.* **2004**, *23* (10), 2175−2184.
(20) Cook, J. D.; Lee, J. E. The Secret Life of Viral Entry Glycoproteins: Moonlighting in Immune Evasion. *PLoS Pathog.* **2013**, *9* (5), e1003258.
(21) Müller, D. J.; Dumitru, A. C.; Lo Giudice, C.; Gaub, H. E.; Hinterdorfer, P.; Hummer, G.; De Yoreo, J. J.; Dufrêne, Y. F.; Alsteens, D. Atomic Force Microscopy-Based Force Spectroscopy and Multiparametric Imaging of Biomolecular and Cellular Systems. *Chem. Rev.* **2021**, *121* (19), 11701−11725.
(22) Zhang, Q.; Tian, F.; Wang, F.; Guo, Z.; Cai, M.; Xu, H.; Wang, H.; Yang, G.; Shi, X.; Shan, Y.; Cui, Z. Entry Dynamics of Single Ebola Virus Revealed by Force Tracing. *ACS Nano* **2020**, *14* (6), 7046−7054.
(23) Yuan, S.; Cao, L.; Ling, H.; Dang, M.; Sun, Y.; Zhang, X.; Chen, Y.; Zhang, L.; Su, D.; Wang, X.; Rao, Z. TIM-1 Acts a Dual-Attachment Receptor for Ebolavirus by Interacting Directly with Viral GP and the PS on the Viral Envelope. *Protein & Cell* **2015**, *6* (11), 814−824.
(24) Evans, E. A.; Calderwood, D. A. Forces and Bond Dynamics in Cell Adhesion. *Science* **2007**, *316*, 1148−1153.
(25) Evans, E.; Ritchie, K. Dynamic Strength of Molecular Adhesion Bonds. *Biophys. J.* **1997**, *72* (4), 1541−1555.
(26) Dragovich, M. A.; Fortoul, N.; Jagota, A.; Zhang, W.; Schutt, K.; Xu, Y.; Sanabria, M.; Moyer, D. M.; Moller-Tank, S.; Maury, W.; Zhang, X. F. Biomechanical Characterization of TIM Protein−Mediated Ebola Virus−Host Cell Adhesion. *Sci. Rep.* **2019**, *9* (1), 267.
(27) Evans, E.; Williams, P. *Dynamic Force Spectroscopy*; Springer Berlin Heidelberg: Berlin, Heidelberg, 2002; pp 145−204.
(28) Williams, P. M. Analytical Descriptions of Dynamic Force Spectroscopy: Behaviour of Multiple Connections. *Anal. Chim. Acta* **2003**, *479* (1), 107−115.
(29) Rankl, C.; Kienberger, F.; Wildling, L.; Wruss, J.; Gruber, H. J.; Blaas, D.; Hinterdorfer, P. Multiple Receptors Involved in Human Rhinovirus Attachment to Live Cells. *Proc. Natl. Acad. Sci. U. S. A.* **2008**, *105* (46), 17778.
(30) Baumgartner, W.; Gruber, H. J.; Hinterdorfer, P.; Drenckhahn, D. Affinity of Trans-Interacting VE-Cadherin Determined by Atomic Force Microscopy. *Single Molecules* **2000**, *1* (2), 119−122.
(31) Gramberg, T.; Soilleux, E.; Fisch, T.; Lalor, P. F.; Hofmann, H.; Wheeldon, S.; Cotterill, A.; Wegele, A.; Winkler, T.; Adams, D. H.; Pöhlmann, S. Interactions of LSECtin and DC-SIGN/DC-SIGNR with Viral Ligands: Differential PH Dependence, Internalization and Virion Binding. *Virology* **2008**, *373* (1), 189−201.
(32) Kuroda, M.; Fujikura, D.; Nanbo, A.; Marzi, A.; Noyori, O.; Kajihara, M.; Maruyama, J.; Matsuno, K.; Miyamoto, H.; Yoshida, R.; Feldmann, H.; Takada, A. Interaction between TIM-1 and NPC1 Is Important for Cellular Entry of Ebola Virus. *J. Virol.* **2015**, *89* (12), 6481−6493.
(33) Alsteens, D.; Newton, R.; Schubert, R.; Martinez-Martin, D.; Delguste, M.; Roska, B.; Müller, D. J. Nanomechanical Mapping of First Binding Steps of a Virus to Animal Cells. *Nat. Nanotechnol.* **2017**, *12* (2), 177−183.
(34) Rasmussen, A. L. Host Factors in Ebola Infection. *Annu. Rev. Genom. Hum. Genet.* **2016**, *17* (1), 333−351.
(35) Nanbo, A.; Imai, M.; Watanabe, S.; Noda, T.; Takahashi, K.; Neumann, G.; Halfmann, P.; Kawaoka, Y. Ebolavirus Is Internalized into Host Cells via Macropinocytosis in a Viral Glycoprotein-Dependent Manner. *PLoS Pathog.* **2010**, *6* (9), e1001121.
(36) Wang, H.; Shi, Y.; Song, J.; Qi, J.; Lu, G.; Yan, J.; Gao, G. F. Ebola Viral Glycoprotein Bound to Its Endosomal Receptor Niemann-Pick C1. *Cell* **2016**, *164* (1), 258−268.
(37) Carette, J. E.; Raaben, M.; Wong, A. C.; Herbert, A. S.; Obernosterer, G.; Mulherkar, N.; Kuehne, A. I.; Kranzusch, P. J.; Griffin, A. M.; Ruthel, G.; Cin, P. D.; Dye, J. M.; Whelan, S. P.; Chandran, K.; Brummelkamp, T. R. Ebola Virus Entry Requires the Cholesterol Transporter Niemann−Pick C1. *Nature* **2011**, *477* (7364), 340−343.

https://doi.org/10.1021/acs.nanolett.1c04677
Nano Lett. XXXX, XXX, XXX−XXX